

A *WISE* View of *IRAS* Debris Disks: Revising the Dust Properties

Qiong Liu¹

Department of Physics, Guizhou University, Guiyang 550025, China; qliu1@gzu.edu.cn

Received 20xx month day; accepted 20xx month day

Abstract Debris disks around stars are considered as components of planetary systems. Constrain the dust properties of these disks can give crucial information to formation and evolution of planetary systems. As an all-sky survey, *Infrared Astronomical Satellite (IRAS)* gave great contribution to the debris disk searching which discovered the first debris disk host star (Vega). The *IRAS*-detected debris disk sample published by Rhee (Rhee et al. 2007) contains 146 stars with detailed information of dust properties. While the dust properties of 45 of them still can not be determined due to the limitations with the *IRAS* database (have *IRAS* detection at 60 μm only). Therefore, using more sensitivity data of *Wide-field Infrared Survey Explorer (WISE)*, we can better characterize the sample stars: For the stars with *IRAS* detection at 60 μm only, we refit the excessive flux densities and obtain the dust temperatures and fractional luminosities; While for the remaining stars with multi-bands *IRAS* detections, the dust properties are revised which show that the dust temperatures were over estimated in high temperatures band before. Moreover, we identify 17 stars with excesses at the *WISE* 22 μm which have smaller distribution of distance from Earth and higher fractional luminosities than the other stars without mid-infrared excess emission. Among them, 15 stars can be found in previous works.

Key words: (stars:) circumstellar matter — protoplanetary disks —infrared: stars

1 INTRODUCTION

Debris disks are almost dust-dominated and surround their stars with a wide age range (Hughes et al. 2018). The dust is usually not primordial because its lifetime was much shorter than the stellar age (Wyatt 2018). Debris disks are considered as planetary systems components or protoplanetary disks descendants, which provides a wealth of valuable information on evolution of circumstellar disks and planet formation outcome (Wyatt et al. 2017).

Since *IRAS* first discovered Vega with debris disk in 1984 (Auman et al. 1984), attempts of searching debris disk candidates are never stop. The most effective way of searching debris disk is to detect the infrared

and reaches a thermal equilibrium under stellar radiation, then it will re-emits the light absorbed from the host star at IR to sub-millimeter (Krivov 2010).

Up to now, many hundreds of debris disks have been discovered (Wyatt 2018). They are based on five satellites as follows: *IRAS* (Rhee et al. 2007; Mannings & Barlow 1998), *Infrared Space Observatory (ISO)* (Oudmaijer et al. 1992; Kessler et al. 1996; Abraham et al. 1999; Fajardo et al. 1999; Habing et al. 1999; Spangler et al. 2001; Decin et al. 2003), *Spitzer* (Chen et al. 2005; Rieke et al. 2005; Kim et al. 2005; Su et al. 2006; Beichman et al. 2006; Moór et al. 2006; Bryden et al. 2006; Siegler et al. 2007; Rebull et al. 2008; Moór et al. 2011; Wu et al. 2012; Chen et al. 2014; Mittal et al. 2015; Ballering et al. 2018), *Herschel* (Matthews et al. 2010; Eiroa et al. 2013; Dodson-Robinson et al. 2016; Vican et al. 2016; Sibthorpe et al. 2018), and *AKARI* (Fujiwara et al. 2013; Liu et al. 2014; Ishihara et al. 2017). Among these surveys, *IRAS* and *AKARI* are all-sky surveys and the other three (*Spitzer*, *ISO* and *Herschel*) are not. Though with much smaller area covering, the latter three missions have much better sensitivities and spatial resolutions so that they can detect more faint disks.

However, *IRAS* and *AKARI* still have their own advantages because of their all-sky area. And although both *IRAS* and *AKARI* are all-sky surveys, the debris disk candidates detected by them are not exactly the same. The debris disk sample of Rhee (Rhee et al. 2007) detected by *IRAS* contains 146 stars with debris disk candidates via cross-correlating the *IRAS* Point Source Catalog (PSC) and Faint Source Catalog (FSC) with the *Hipparcos* main sequence star catalog. And the debris disk sample of Liu (Liu et al. 2014) detected by *AKARI* contains 72 stars debris disk candidates via cross-correlating the *AKARI/Far-Infrared Surveyor* (Kawada et al. 2007) All-Sky Survey Bright Source Catalogue (AKARIBSC, Yamamura et al. 2010) with the *Hipparcos* main sequence star catalog. Among these two samples, 27 stars are in common although they have the similar sensitivity (*IRAS* at 60 μm band and *AKARI/FIS* at 90 μm). Most of the sources in Rhee's sample cannot be detected by *AKARI/FIS* because of its shallow limit. So Rhee's sample still has its own value.

The sample of Rhee gives dust properties of debris disks including dust temperature, fractional luminosity and dust mass. It presents a good sample for other works, such as follow up observations of debris disks (*Herschel*: Marshall et al. 2013; Vican et al. 2016, *Spitzer*: Chen et al. 2014; Mittal et al. 2015, *ALMA*: Booth et al. 2019 and Submillimeter: Bulger et al. 2013; Holland et al. 2017); debris disks around A-type stars (Greaves et al. 2016; Welsh & Montgomery 2018; Moór et al. 2017); Individual disk research (Fujiwara et al. 2009; Borgniet et al. 2014; Hung et al. 2015; Su et al. 2015; Konopacky et al. 2016; Geiler et al. 2019). Moreover, this sample focuses on debris disks evolution which gives great guidance to evolution works of other people (Wyatt et al. 2007; Moór et al. 2011; Vican & Schneider 2014). And this sample is also helpful to other statistical works: metallicity (Maldonado et al. 2012), binaries (Rodríguez & Zuckerman 2012), Kuiper Belts (Nilsson et al. 2010) and so on.

However, the dust properties of 45 of them still cannot be determined due to the limitations with the *IRAS* database: these stars have only *IRAS* 60 μm detection. This limitation can be broken through with more sensitivity observation data of *Wide-field Infrared Survey Explorer (WISE)*. Many studies have used *WISE* to search for IR excess stars (Cotten & Song 2016; Wu et al. 2013, 2016). *WISE* makes an all-sky survey at four IR bands with *W1* at 3.4 μm , *W2* at 4.6 μm , *W3* at 12 μm and *W4* at 22 μm . The angular resolutions

bands are better than 0.08, 0.11, 1 and 6 mJy. For high SNR sources, the astrometry precision is better than $0''.15$ (Wright et al. 2010). The flux densities of *W*1 and *W*2 can be used to test the fitting quality of model spectra. And the flux densities of *W*3 and *W*4 can be used to fit the dust components and revise the properties.

This paper has refitted the SEDs of Rhee’s sample stars and refitted the excessive flux densities with *WISE* all-sky source catalog and *IRAS* catalog to revise the dust properties and get Mid-IR excess information. The sample and photosphere emission are described in Section 2 and results and analysis including the properties of debris disks and hosting stars as well as *WISE* $22\mu\text{m}$ excess are presented in Section 3. I will discuss the revised dust properties and Mid-IR excess sample in Section 4 and draw the summary in Section 5.

2 THE SAMPLE AND PHOTOSPHERE EMISSION

2.1 The Sample

The sample used in this work is debris disks of 146 stars within 120 pc of Earth detected by *IRAS* (Rhee et al. 2007), which cross-correlate the *IRAS* Point Source Catalog (PSC) and Faint Source Catalog (FSC) with the *Hipparcos* main sequence star catalog. *IRAS* makes an all-sky survey at four bands centered at 12, 25, 60, and $100\mu\text{m}$ (Neugebauer et al. 1984). The *Hipparcos* main sequence star catalog has more than 110,000 stars with the information of photometry and astrometry for the nearby stars (Bessell 2000).

All stars have debris disks around, which are identified by excesses at *IRAS* $60\mu\text{m}$ as described in the paper of Rhee. We will check these results in the Section 3. Note that 3 stars were removed from the sample: 2 pre-main-sequence stars (HIP 53911, HIP 77542) and 1 star (HIP 19704) with a detection at $60\mu\text{m}$ flux quality of 1 (which means the flux quality is not reliable). The sample has 143 stars left over.

2.2 The Photosphere Emission

It is essential to obtaining the 143 sample stars’ photosphere flux densities in order to identify and measure the IR excess strength (Bryden et al. 2006). To construct the SEDs, we collected the optical data (*B* and *V* from the *Hipparcos* satellite measurements) to near-infrared (NIR) absolute photometric data (*JHK_s* from Two Micron All Sky Survey (2MASS) catalog) for all sample stars (Skrutskie et al. 2006) and converted these observed magnitudes into flux density (Janskys) by using the zero magnitudes in Cox et al. 2000. The photometry of the sample stars are listed in Table 1. Then we use Kurucz’ models (ATLAS9, Castelli et al. 2004) to fit the stellar SEDs as our previous work do (Liu et al. 2014). The best model was selected out with the minimum χ^2 which are presented in Table 1.

3 RESULTS AND ANALYSIS

With the best-fit Kurucz model, we can estimate the flux densities of stellar photosphere in the corresponding *WISE* and *IRAS* bands. We check the *IRAS* excesses of all 143 sample stars by using the criterion $[F_{IRAS} - F_{phot}] / \sigma_{IRAS} > 3.0$, where F_{IRAS} is the *IRAS* flux densities; F_{phot} is the predicted photospheric flux densities of corresponding bands; and σ_{IRAS} is the uncertainties of the *IRAS* flux densities in corresponding

3.1 WISE 22 μm Excess

The observation data of *WISE* will be used to search Mid-IR excess objects. All 143 stars are covered by *WISE*. While our previous work showed that the model fluxes at *WISE* 12 and 22 μm have the systematical uncertainties σ_{sys} with $\sigma_{w3} = 0.06$ and $\sigma_{w4} = 0.13$ (Liu et al. 2014). Therefore, the systematical uncertainty should be considered to the uncertainties of *WISE* all bands σ_{WISE} with $\sigma_{WISE} = \text{sqr}t(\sigma_{obs}^2 + \sigma_{sys}^2)$, where σ_{obs} means the observational uncertainties of *WISE*. Note that 3 stars (HIP 70952, HIP 71284, HIP 74946) were removed from the sample with $[F_{w4obs} - F_{w4phot}] < -1 * \sigma_{w4}$ where F_{w4obs} is the *WISE* 22 μm flux density and F_{w4phot} is the predicted photospheric flux density at 22 μm band. Therefore, there are 140 stars left in our sample for further discussion. These 140 stars's *WISE* magnitudes information can be seen from Table 1.

The flux densities of *W1* and *W2* can be used to test the fitting quality of model spectra. And the flux densities of *W3* and *W4* can be used to fit the dust components and revise the dust properties of the stars in Rhee et al. (2007). We can estimate the Mid-IR excesses at *WISE* 22 μm in the same way as 60 μm excess shown:

$$[F_{w4obs} - F_{w4phot}] / \sigma_{w4} > 3.0,$$

We identify 31 stars with excesses at the 22 μm by applying this criterion. While this criterion is affected by the *IRAS* 100 μm background, whose level should be lower than 5 MJy/sr as Kennedy & Wyatt 2012 and Wu et al. 2013 shown. We check the 31 μm excess stars and find indeed there are 14 stars may be affected. So there are only 17 stars left after this cut. Mid-IR excess stars are thought to have co-existence of hot and cold dust components just like our solar system. These 17 stars are putted into Mid-IR excess sample which are listed in Table 5. At the following sections, I will discuss this two sub-samples: Mid-IR excess sample and Non Mid-IR excess sample.

3.2 Properties of Debris Disk Host stars

In this subsection, I will study the stellar properties of debris disk hosts including color, distance from the Earth and location on the H-R diagram. Debris disk host stars are more inclined to early type stars as Rhee et al. (2007) pointed out which can be seen from the figure of sample stars function distribution of the distance from Earth and B-V. We re-draw the figure and mark the Mid-IR excess objects in red dots as Figure 1 shown. From the figure, we can see Mid-IR excess sample has smaller distribution of distance from Earth (29.2 pc to 103.5 pc) than Non Mid-IR excess sample stars (3.2 pc to 117.8 pc). Note that there are only 17 Mid-IR excess stars, the sample is so small that may lead to a false distribution trend.

3.3 Dust Properties

In this subsection, I will study the dust properties including the dust temperatures and fractional luminosities

3.3.1 Dust Temperatures

Debris disks usually consist of a single narrow ring which reach thermal equilibrium in the field of stellar radiation as previous studies suggested (Backman & Paresce 1993). Rhee et al. (2007) used the blackbody model with single-temperature to fit the dust component and obtained dust temperature T for each star.

Since *IRAS* sample of Rhee is based on solely *IRAS*, the dust properties of 45 objects in their sample still can not be determined due to the limitations with the *IRAS* database (have *IRAS* detection at 60 μm only). They set the dust temperature to 85 K so the peak will fall at 60 μm . According to the number of the *IRAS* detected bands, I divide the 140 stars sample to 2 groups:

- (1) Group I contains 45 stars with only *IRAS* 60 μm detection;
- (2) Group II contains the remaining 95 stars with multi-bands *IRAS* detections.

The excessive flux densities are fitted in IR bands including 60, 100 μm of *IRAS* and 12, 22 μm of *WISE* with a blackbody model of single temperature. The SED fittings of 4 stars as an example are presented in Figure 2. From SED fittings, the dust temperatures can be derived with group I stars listed in Table 6 and Group II stars listed in Table 7. From the figure, one can easily see that our fitting results are better than Rhee's because of the addition of new *WISE* data.

3.3.2 Fractional Luminosities

From the SED fitting, we can also estimate the fractional luminosity f which is used to characterize the disk's effective optical depth. The fractional luminosity f is calculate by divided the IR luminosity of debris disk to the stellar luminosity (Wyatt 2008),

$$f = L_{\text{ir}}/L_{\star} \quad (1)$$

where L_{\star} is the stellar luminosity estimated by the best model of SED fitting. The IR luminosity L_{ir} is calculated from the blackbody model of fitted IR. The calculated fractional luminosities for all sample stars are listed in Table 6 and Table 7 as well.

4 DISCUSSION

In this section, I will first give my discussion on revising the dust properties including dust temperatures and fractional luminosities. And then, I will discuss the Mid-IR excess sample.

4.1 Revising the Dust Temperatures

The revised dust temperature can be seen in Table 6 and Table 7. For Group I stars, we can get the dust temperatures which were set to 85 K in Rhee et al. 2007. And for Group II stars, even they have multi-bands *IRAS* detections, the dust temperatures of ours are well determined than that in Rhee et al. 2007 because of the much better sensitivity in the Mid-IR of *WISE* in comparison with *IRAS*.

The difference of dust temperatures between Rhee et al. (2007) and ours is shown in Figure 3. From Figure 3, we can see the dust temperatures of Group II stars are over estimated in high temperatures band. While in lower temperature band (<100 K), dust temperatures have a part under estimated and a part over

4.2 Revising the Fractional Luminosities

The differences of fractional luminosities f between Rhee et al. (2007) and ours are shown in Figure 4. It is obvious that the fractional luminosities of Group I stars are high estimated by Rhee due to the high estimated dust temperatures which can be seen from the left panel of Fig. 4. While for Group II stars, the fractional luminosities show no obvious favoritism with a part under estimated and a part over estimated which can be seen from the right panel of Fig. 4. However, for the Mid-IR excess sample stars in this group, fractional luminosities of mine are almost the same as Rhee et al. (2007). It is most likely because they have plenty of IR excess data to do blackbody fittings.

Whether in Group I or Group II, Mid-IR sample stars have high fractional luminosities than Non Mid-IR sample stars which imply that the stars with higher fractional luminosities may have higher probability of having warm dust component.

4.3 Mid-IR Excess Sample (*WISE* 22 μm)

From Section 3, Mid-IR excess sample contains 17-stars with *WISE* 22 μm excesses. Such stars with Mid-IR excess emission may have terrestrial planets (Padgett & Stapelfeldt 2016).

Up to now, a few hundreds of warm disks with Mid-IR excess have been discovered with *Spitzer*, *AKARI* and *WISE* (Meyer et al. 2008; Fujiwara et al. 2010; Fujiwara & Ishihara et al. 2010; Olofsson et al. 2012; Ribas et al. 2012; Fujiwara et al. 2013; Wu et al. 2012, 2013; Liu et al. 2014; Ishihara et al. 2017; Ballering et al. 2018), and such disks' incidence decreases very rapidly with increasing stellar ages (Urban et al. 2012).

What is the cause of the warm component? For most warm debris disks, the Mid-IR excesses could be explained by giant impact stages (about 100 Myr) (Genda et al. 2015). They found that, after a giant impact, the IR excess is sometimes almost 10 times higher than the stellar IR flux.

In Mid-IR excess sample, 15 stars can be found in previous work as Table 5 column 3 shown. Note [that](#) maybe the remaining 2 stars can be seen in the other work elsewhere.

5 SUMMARY

This paper has refitted the SEDs of the sample stars with the Kurucz' models and refitted the excessive flux densities with *WISE* and *IRAS* all sky catalogs. we obtain the dust temperatures of Group I stars with only 60 μm data which can not determined in previous study of Rhee. And for Group II stars, even they have *IRAS* multi-bands detections, the dust temperatures of ours are well determined than that in Rhee et al. 2007 because of the much better sensitivity in the Mid-IR of *WISE* in comparison with *IRAS*. From the revised dust properties, we can see that the dust temperatures of Group II stars were over estimated in high temperatures band before and the fractional luminosities of Group I stars were high estimated.

Moreover, we identify 17 stars with *WISE* 22 μm excess and discuss the difference from Non Mid-IR sample. Disks around the Mid-IR sample stars appear to be more bright and with higher dust temperatures. We hope these revision of dust properties can give some guidance to the follow-up works.

Acknowledgements I am grateful to the anonymous referee for his/ her comments that improved the paper.

work is based on the sample of Rhee and makes use of data products from many telescopes: *WISE* (a joint project of the University of California, Los Angeles, and the Jet Propulsion Laboratory/California Institute of Technology), *Hipparcos* (the primary result of the Hipparcos space astrometry mission, undertaken by the European Space Agency) and *2MASS* (a joint project of the University of Massachusetts and the Infrared Processing and Analysis Center /California Institute of Technology). This research makes use of ATLAS9 model and the SIMBAD database, operated at the CDS, Strasbourg, France. And this work makes use of the NASA/IPAC Infrared Science Archive, which is operated by the Jet Propulsion Laboratory, California Institute of Technology, under contract with the National Aeronautics and Space Administration.

References

- Abraham, P., Leinert, C., Burkert, A., Lemke, D., Henning, T. 1999, *A&A*, 338, 91 [2](#)
- Aumann, H. H., et al. 1984, *ApJ*, 278, L23 [1](#)
- Backman, D. E., & Paresce, F. 1993, in *Protostars and Planets III*, ed. V. Mannings, A. P. Boss, & S. S. Russell (Tucson: Univ. Arizona Press), 1253 [5](#)
- Ballering, N. P., Rieke, G. H., Su, K. Y. L., et al. 2018, *VizieR Online Data Catalog*, *J/ApJ/845/120* [2](#), [6](#), [18](#)
- Beichman, C. A., Bryden, G., Stapelfeldt, K. R. et al. 2006, *ApJ*, 652, 1674 [2](#)
- Bessell, M. 2000, *PASP*, 112, 961 [3](#)
- Booth, M., Matrà, L., Su, K. Y. L., et al. 2019, *MNRAS*, 482, 3443
- Borgniet, S., Boisse, I., Lagrange, A.-M., et al. 2014, *A&A*, 561, A65 [2](#)
- Bryden, G. et al. 2006, *ApJ*, 636, 1098 [2](#)
- Bulger, J., Hufford, T., Schneider, A. et al. 2013, *A&A*, 556, A119 [2](#), [3](#)
- Castelli, F. & Kurucz, R. L. 2004, *arXiv:astro-ph/0405087* [2](#)
- Chen, C. H., Patten, B. M., Werner, M. W., et al. 2005, *ApJ*, 634, 1372 [3](#)
- Chen, C.H., Mittal, T., Kuchner, M., et al. 2014, *ApJS*, 211, 25 [2](#)
- Cotten, T.H. & Song, I. 2016, *ApJS*, 225, 15 [2](#)
- Cox, A. N., ed. 2000, *Allen's Astrophysical Quantities* [2](#)
- Decin, G., Dominik, C., Waters, L. B. F. M., Waelkens, C. 2003, *ApJ*, 598, 636 [3](#)
- Dodson-Robinson, S. E., Su, K. Y. L., Bryden, G., et al. 2016, *ApJ*, 833, 183 [2](#)
- Eiroa, C., Marshall, J. P. et al. 2013, *A&A*, 555, 11 [2](#)
- Fajardo-Acosta, S. B., Stencel, R. E., Backman, D. E., Thakur, N. 1999, *ApJ*, 520, 215 [2](#)
- Fujiwara, H., Yamashita, T., Ishihara, D., et al. 2009, *ApJ*, 695, L88 [2](#)
- Fujiwara, H., Onaka, K., et al. 2010, *ApJ*, 714, 152 [2](#)
- Fujiwara, H., Ishihara, D., et al. 2010, *cosp*, 38, 2470 [6](#)
- Fujiwara, H., Ishihara, D., et al. 2013, *A&A*, 550, 45 [6](#)
- Geiler, F., Krivov, A. V., Booth, M., et al. 2019, *MNRAS*, 483, 332 [2](#), [6](#), [18](#)
- Genda, H., Kobayashi, H., & Kokubo, E. 2015, *ApJ*, 810, 136 [2](#)
- Greaves, J. S., Holland, W. S., Matthews, B. C., et al. 2016, *MNRAS*, 461, 3910 [6](#)
- Habing, H., Dominik, C., Jourdain de Muizon, M., et al. 1999, *Nature*, 401, 456 [2](#)

- Hughes, A. M., Ducheâne, G. & Matthews, B. C. 2018, *ARA&A*, 56, 13 [2](#)
- Hung, L. W., Fitzgerald, M. P., Chen, C. H., et al. 2015, *ApJ*, 802, 138 [1](#)
- Ishihara, D., Takeuchi, N., Kobayashi, H., et al. 2017, *A&A*, 601, A72 [2](#)
- Kawada, M., Baba, H., et al. 2007, *PASJ*, 59, 389 [2](#), [6](#), [18](#)
- Kennedy, G. M., & Wyatt, M. C. 2012, *MNRAS*, 426, 91 [2](#)
- Kessler, M. F., Steinz, J. A., et al. 1996, *A&A*, 315, 27 [4](#)
- Kim, J. S., Hings, D. C., Rivinius 2005, *ApJ*, 632, 659 [2](#)
- Konopacky, Q. M., Rameau, J., Duchêne, G., et al. 2016, *ApJ*, 829, L4 [2](#)
- Krivov, A. V. 2010, *Research in Astron. Astrophys. (RAA)*, 10, 383 [2](#)
- Liu, Q., Wang, T. G. & Jiang, P. 2014, *AJ*, 148, 3 [2](#)
- Marshall, J. P., Krivov, A. V., del Burgo, C., et al. 2013, *A&A*, 557, A58 [2](#), [3](#), [4](#), [6](#), [18](#)
- Matthews, B. C., Sibthorpe, B., Kennedy, G. et al. 2010, *A&A*, 518, 135 [2](#)
- Maldonado, J., Eiroa, C., Villaver, E., et al. 2012, *A&A*, 541, A40 [2](#)
- Mannings, V., Barlow, M. J. 1998, *ApJ*, 497, 330 [2](#)
- Meyer, M. R., et al. 2008, *ApJ*, 673, L181 [2](#)
- Mittal, T., Chen, C.H., Jang-Condell, H., et al. 2015, *ApJ*, 798, 87 [6](#)
- Moór, I., Abraham, P., Derekas, A. et al. 2006, *ApJ*, 644, 525 [2](#)
- Moór, I., Pascucci, A. et al. 2011, *ApJS*, 193, 4 [2](#)
- Moór, A., Curé, M., Kóspál, Á., et al. 2017, *ApJ*, 849, 123 [2](#)
- Neugebauer, G., Habing, H. J., et al. 1984, *ApJ*, 278, 1 [2](#)
- Nilsson, R., Liseau, R., Brandeker, A., et al. 2010, *A&A*, 518, A40 [3](#)
- Olofsson, J., Juhaász, A. et al. 2012, *A&A*, 542, 90 [2](#)
- Oudmaijer, R. D., van der Veen, W. E. C. J. et al. 1992, *A&A*, 96, 625 [6](#)
- Padgett, D., & Stapelfeldt, K. 2016, *Young Stars & Planets Near the Sun*, 175 [2](#)
- Rebull, L. M., et al. 2008, *ApJ*, 681, 1484 [6](#)
- Rhee, J. H., Song, I. R., Zuckerman, B., McElwain, M. 2007, *ApJ*, 660, 1556 [2](#)
- Ribas, A., Meriñ, B. et al. 2012, *A&A*, 541, 38 [1](#), [2](#), [3](#), [5](#), [6](#)
- Rieke, G. H., Young, E. T., Engelbracht, C. W., et al. 2004, *ApJS*, 154, 25 [6](#)
- Rieke, G. H., et al. 2005, *ApJ*, 620, 1010
- Rodriguez, D. R., & Zuckerman, B. 2012, *ApJ*, 745, 147 [2](#)
- Sibthorpe, B., Kennedy, G. M., Wyatt, M. C., et al. 2018, *MNRAS*, 475, 3046 [2](#)
- Siegler, N., Muzerolle, J., Young, E. T., Rieke, G. H., Mamajek, E. E., Trilling, D. E., Gorlova, N., & Su, K. Y. L. 2007, *ApJ*, 654, 580 [2](#)
- Skrutskie, M. F., Cutri, R. M., Weinberg, M. D. et al. 2006, *AJ*, 131, 1163 [2](#)
- Spangler, C., et al. 2001, *ApJ*, 555, 932S [3](#)
- Su, K. Y. L., Rieke, G. H., Stansberry, J. A., Bryden, G. et al. 2006, *ApJ*, 653, 675 [2](#)
- Su, K. Y. L., Morrison, S., Malhotra, R., et al. 2015, *ApJ*, 799, 146 [2](#)
- Urban, L. E., Rieke, G. et al. 2012, *ApJ*, 750, 98 [2](#)
- Vican, L., & Schneider, A. 2014, *ApJ*, 780, 154 [6](#)

- Vican, L., Schneider, A., Bryden, G., et al. 2016, *ApJ*, 833, 263 [2](#)
- Welsh, B. Y., & Montgomery, S. L. 2018, *MNRAS*, 474, 1515 [2](#)
- Werner, M.W., Roellig, T. L., Low, F. J., et al. 2004, *ApJS*, 154, 1 [2](#)
- Wright, E. L., et al. 2010, *AJ*, 140, 1868
- Wu, C. J., Wu, H., Lam, M. I., et al. 2013, *ApJS*, 208, 29 [3](#)
- Wu, C. J., Wu, H., Liu, K., et al. 2016, *Research in Astron. Astrophys. (RAA)*, 16, 102 [2](#), [4](#), [6](#), [18](#)
- Wu, H., Wu, C. J., Cao, C. 2012, *Research in Astron. Astrophys. (RAA)*, 12, 513 [2](#)
- Wyatt, M. C., Smith, R., Su, K. Y. L., et al. 2007, *ApJ*, 663, 365 [2](#), [6](#)
- Wyatt, M. C. 2008, *ARA&A*, 46, 339 [2](#)
- Wyatt, M. C., Bonsor, A., Jackson, A.P., et al. 2017, *MNRAS*, 464, 3385 [5](#)
- Wyatt, M. C. 2018, *Handbook of Exoplanets*, 146 [1](#)
- Yamamura, S., et al. 2010, *cosp*, 38, 2496Y [1](#), [2](#)
- [2](#)

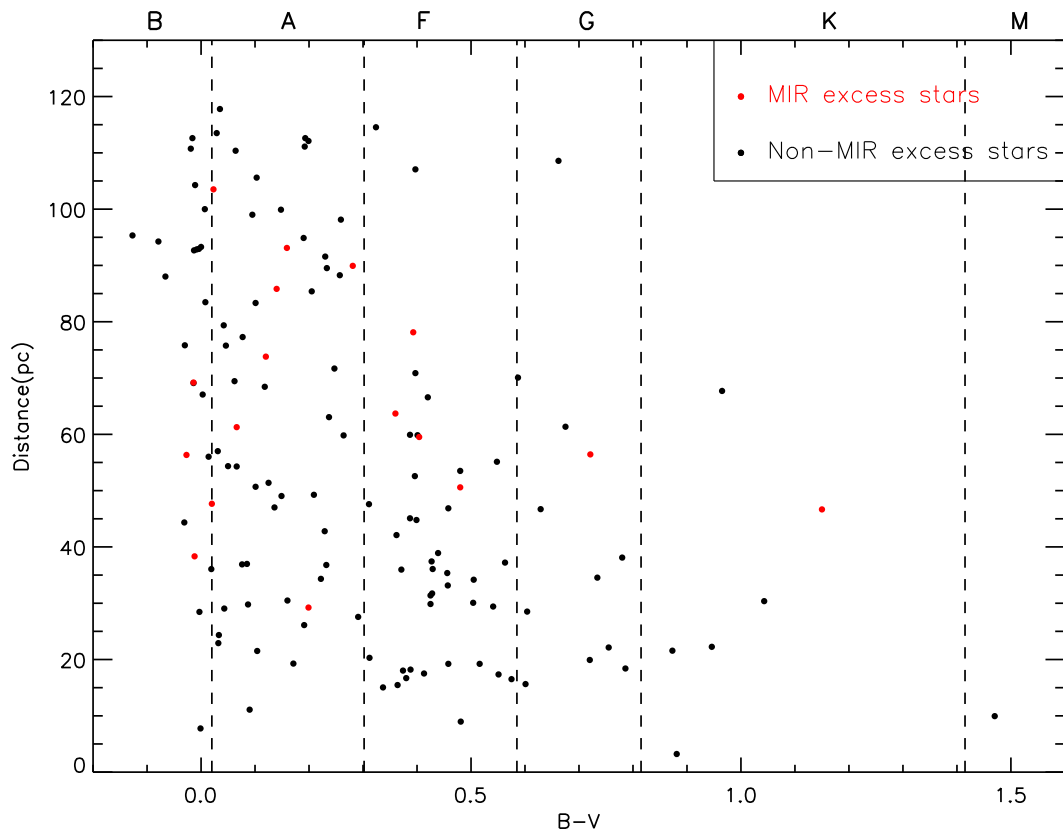


Fig. 1: Distribution of Mid-IR excess sample and Non Mid-IR excess sample stars in distance from Earth as a function of B-V.

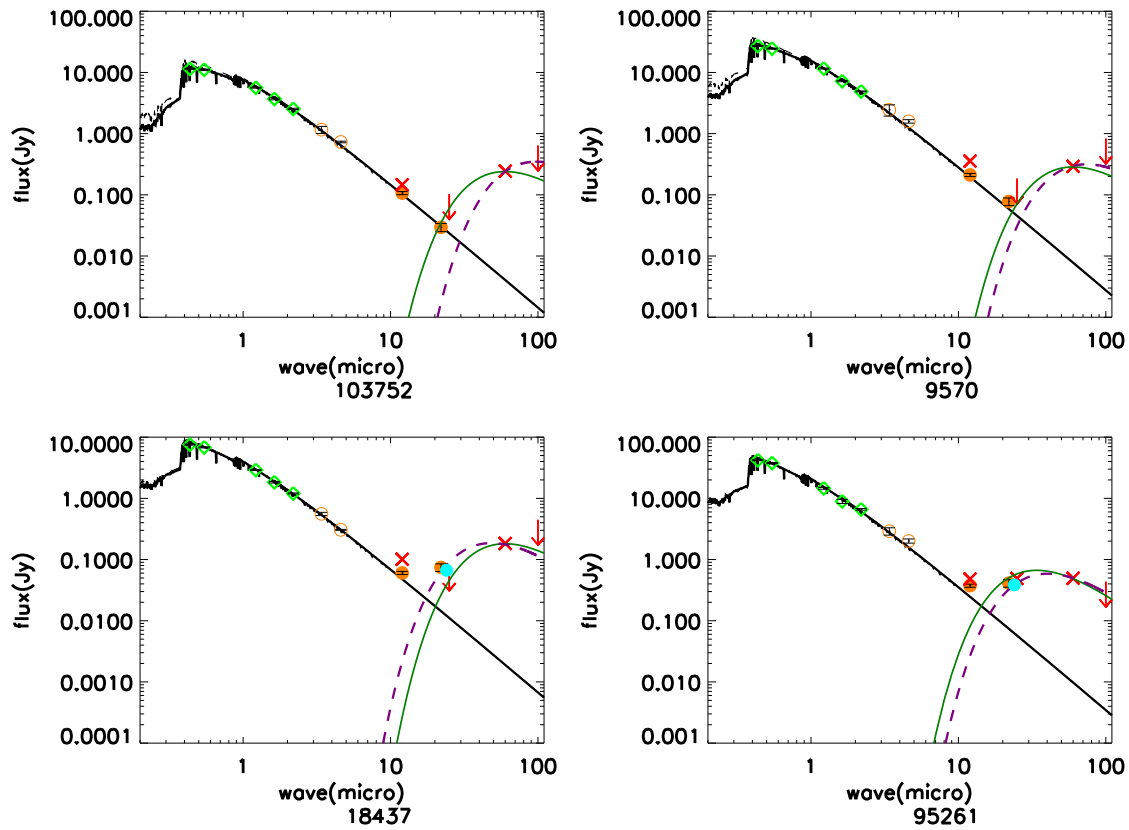


Fig. 2: SEDs for 4 IR excess stars. The photospheric models and the disk models are shown as solid black and dotted purple lines, respectively. The green solid lines are the disk models of Rhee. The different symbols represent the different data sets: green diamonds, BVJHK; red, IRAS; cyan filled dots, Spitzer; orange filled dots, WISE without saturations; and orange hollow circles, WISE with saturations.

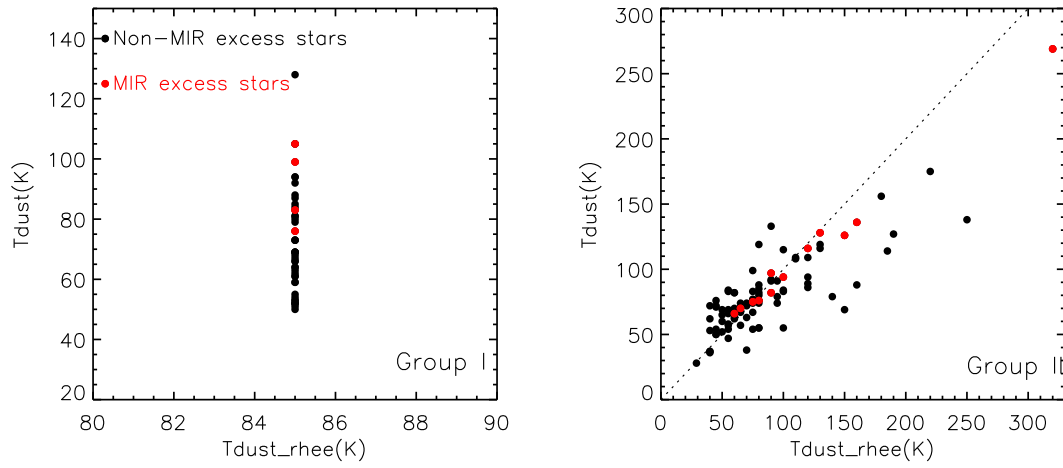


Fig. 3: The differences of dust temperatures between Rhee et al. (2007) and ours. Group I and Group II stars are shown in the left and right panels, respectively. The different symbols represent the different sub-sample stars: red filled dots are MIR excess stars and black filled dots are the Non-MIR excess stars.

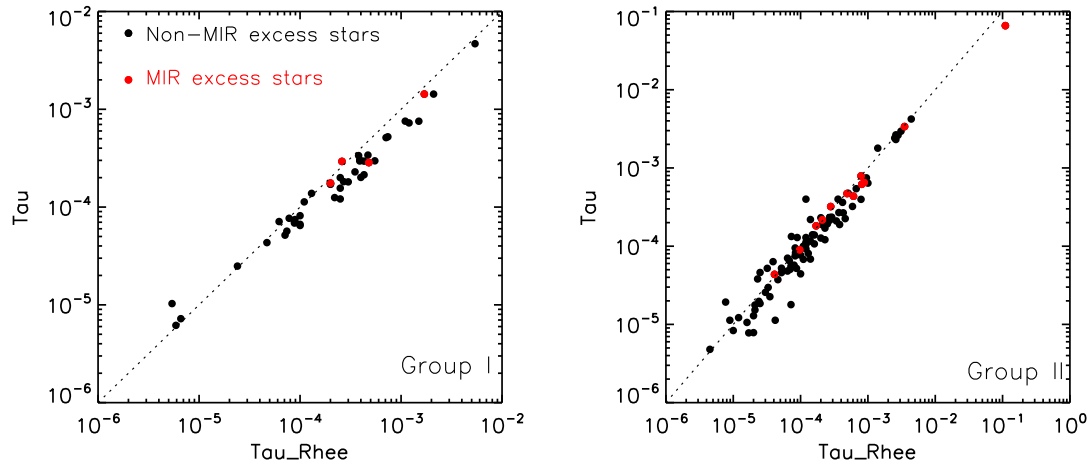


Fig. 4: The differences of fractional luminosities between Rhee et al. (2007) and ours. Group I and Group II stars are shown in the left and right panels, respectively. The different symbols represent the different sub-sample stars: red filled dots are MIR excess stars and black filled dots are the Non-MIR excess stars.

Table 1: Photometry and Flux Density for the 140 Sample Stars.

| HIP | B | V | J | H | K | w1m | w2m | w3m | w4m | f12 | f25 | f60 | f100 | χ^2 |
|-------|------|------|------|------|------|--------|--------|-------|-------|--------|-------|--------|--------|----------|
| | mag | mag | mag | mag | mag | mag | mag | mag | mag | Jy | Jy | Jy | Jy | |
| 746 | 2.66 | 2.28 | 1.71 | 1.58 | 1.45 | -0.876 | -0.178 | 1.462 | 1.335 | 11.700 | 2.871 | 1.001 | 12.660 | 5.85e-01 |
| 1185 | 7.08 | 6.82 | 6.38 | 6.31 | 6.25 | 6.191 | 6.142 | 6.284 | 6.228 | 0.175 | 0.167 | 0.211 | 0.567 | 4.46e-03 |
| 4267 | 5.78 | 5.80 | 5.74 | 5.80 | 5.80 | 5.801 | 5.734 | 5.825 | 5.454 | 0.193 | 0.149 | 0.174 | 1.309 | 1.00e-03 |
| 5626 | 5.61 | 5.60 | 5.46 | 5.50 | 5.49 | 5.535 | 5.388 | 5.493 | 4.656 | 0.260 | 0.111 | 0.403 | 2.081 | 3.22e-02 |
| 6686 | 2.82 | 2.66 | 2.34 | 2.37 | 2.25 | 0.834 | 0.793 | 2.378 | 2.286 | 4.961 | 1.142 | 0.346 | 6.092 | 2.11e+00 |
| 6878 | 7.17 | 6.66 | 5.69 | 5.49 | 5.42 | 5.443 | 5.256 | 5.441 | 5.321 | 0.310 | 0.112 | 0.285 | 1.045 | 2.60e-01 |
| 7345 | 5.69 | 5.62 | 5.49 | 5.53 | 5.46 | 5.471 | 5.302 | 5.340 | 3.742 | 0.335 | 0.384 | 2.018 | 1.883 | 4.48e+00 |
| 7805 | 8.04 | 7.62 | 6.84 | 6.69 | 6.63 | 6.619 | 6.592 | 6.598 | 6.040 | 0.119 | 0.093 | 0.140 | 0.646 | 1.55e-01 |
| 7978 | 6.07 | 5.52 | 4.79 | 4.40 | 4.34 | 4.171 | 3.913 | 4.220 | 3.954 | 0.814 | 0.282 | 0.815 | 1.075 | 1.04e+01 |
| 8122 | 6.98 | 6.73 | 6.26 | 6.19 | 6.17 | 6.154 | 6.100 | 6.183 | 5.640 | 0.141 | 0.107 | 0.348 | 0.607 | 1.49e-02 |
| 8241 | 5.07 | 5.04 | 4.99 | 5.03 | 4.96 | 4.932 | 4.717 | 4.984 | 4.594 | 0.405 | 0.163 | 0.299 | 0.616 | 4.44e+00 |
| 9570 | 5.53 | 5.50 | 5.35 | 5.38 | 5.33 | 5.246 | 5.078 | 5.345 | 5.069 | 0.356 | 0.184 | 0.293 | 0.829 | 2.03e-01 |
| 10054 | 6.17 | 6.05 | 5.75 | 5.76 | 5.69 | 5.741 | 5.607 | 5.695 | 5.523 | 0.206 | 0.050 | 0.153 | 1.161 | 1.52e-01 |
| 10670 | 4.05 | 4.03 | 3.80 | 3.86 | 3.96 | 3.952 | 3.643 | 3.989 | 3.510 | 1.066 | 0.367 | 0.791 | 0.831 | 2.86e+00 |
| 11360 | 7.19 | 6.79 | 6.03 | 5.86 | 5.82 | 5.814 | 5.646 | 5.778 | 5.269 | 2.130 | 0.868 | 0.441 | 0.663 | 6.70e-01 |
| 11486 | 5.60 | 5.29 | 5.08 | 4.82 | 4.59 | 4.574 | 4.380 | 4.618 | 4.381 | 0.549 | 0.192 | 0.282 | 0.655 | 6.85e+00 |
| 11847 | 7.83 | 7.47 | 6.70 | 6.61 | 6.55 | 6.544 | 6.520 | 6.503 | 4.236 | 0.125 | 0.177 | 0.868 | 0.853 | 8.35e-01 |
| 12361 | 7.17 | 6.78 | 6.11 | 5.97 | 5.92 | 5.955 | 5.799 | 5.904 | 5.406 | 0.157 | 0.086 | 0.304 | 0.768 | 6.26e+00 |
| 12964 | 6.87 | 6.48 | 5.76 | 5.63 | 5.57 | 5.554 | 5.357 | 5.585 | 5.457 | 0.253 | 0.140 | 0.226 | 0.630 | 1.00e-01 |
| 13005 | 9.03 | 8.06 | 6.42 | 5.99 | 5.88 | 5.887 | 5.842 | 5.913 | 5.859 | 0.138 | 0.245 | 0.288 | 1.013 | 1.24e+00 |
| 13141 | 5.35 | 5.25 | 5.14 | 5.16 | 4.97 | 4.963 | 4.748 | 5.012 | 4.781 | 0.414 | 0.097 | 0.164 | 0.490 | 1.66e+00 |
| 14576 | 2.09 | 2.09 | 1.96 | 1.95 | 1.89 | -0.011 | 0.244 | 1.903 | 1.782 | 7.348 | 1.866 | 0.455 | 1.685 | 5.20e-01 |
| 15197 | 5.03 | 4.80 | 4.42 | 4.25 | 4.22 | 4.149 | 3.869 | 4.135 | 4.102 | 0.848 | 0.235 | 0.214 | 1.566 | 4.04e+00 |
| 16449 | 6.50 | 6.38 | 6.16 | 6.12 | 6.10 | 6.097 | 6.045 | 6.115 | 5.372 | 0.173 | 0.101 | 0.595 | 0.636 | 1.04e-01 |
| 16537 | 4.60 | 3.72 | 2.23 | 1.88 | 1.78 | 2.970 | 2.285 | 1.770 | 1.288 | 9.672 | 2.667 | 1.631 | 2.008 | 4.95e+00 |
| 18437 | 6.91 | 6.89 | 6.85 | 6.87 | 6.86 | 6.851 | 6.868 | 6.705 | 5.118 | 0.101 | 0.080 | 0.183 | 0.446 | 1.98e+00 |
| 18859 | 5.90 | 5.38 | 4.71 | 4.34 | 4.18 | 4.146 | 3.926 | 4.289 | 3.882 | 0.982 | 0.247 | 0.287 | 2.242 | 7.76e-02 |
| 18975 | 5.82 | 5.45 | 4.81 | 4.58 | 4.51 | 4.529 | 4.269 | 4.530 | 4.442 | 0.639 | 0.262 | 0.209 | 1.923 | 6.27e-01 |
| 19704 | 7.31 | 6.99 | 6.34 | 6.29 | 6.18 | 6.093 | 5.945 | 6.160 | 6.060 | 0.131 | 0.050 | 0.239 | 0.938 | 1.78e+00 |
| 19893 | 4.57 | 4.26 | 3.68 | 3.47 | 3.51 | 3.487 | 3.188 | 3.497 | 3.399 | 1.661 | 0.441 | 0.321 | 1.000 | 1.07e-01 |
| 20635 | 4.35 | 4.21 | 4.09 | 4.06 | 4.08 | 3.929 | 3.563 | null | 3.830 | 1.115 | 0.310 | 0.353 | 4.666 | 5.30e-04 |
| 21604 | 5.83 | 5.85 | 5.66 | 5.59 | 5.56 | 5.758 | 5.515 | 5.603 | 5.391 | 0.235 | 0.173 | 0.637 | 7.072 | 1.97e-02 |
| 22226 | 8.24 | 7.85 | 7.10 | 6.95 | 6.89 | 6.872 | 6.867 | 6.867 | 6.000 | 0.092 | 0.066 | 0.274 | 0.478 | 1.23e-01 |
| 22439 | 6.73 | 6.27 | 5.38 | 5.20 | 5.08 | 5.102 | 4.927 | 5.146 | 4.997 | 0.387 | 0.091 | 0.191 | 1.011 | 1.14e-01 |
| 22845 | 4.72 | 4.64 | 4.85 | 4.52 | 4.42 | 4.414 | 4.166 | 4.432 | 4.058 | 0.696 | 0.270 | 0.411 | 5.217 | 5.62e+00 |
| 23451 | 8.33 | 8.13 | 7.69 | 7.62 | 7.59 | 7.595 | 7.629 | 6.924 | 3.952 | 0.114 | 0.211 | 1.122 | 1.592 | 1.17e-29 |
| 24528 | 6.90 | 6.76 | 6.50 | 6.43 | 6.43 | 6.408 | 6.371 | 6.357 | 5.589 | 0.144 | 0.060 | 0.108 | 0.510 | 1.18e+00 |
| 25197 | 5.23 | 5.24 | 5.66 | 5.16 | 5.16 | 5.154 | 5.006 | 5.154 | 4.925 | 0.352 | 0.172 | 0.172 | 1.549 | 7.30e+00 |
| 25790 | 6.03 | 5.93 | 5.61 | 5.60 | 5.55 | 5.558 | 5.439 | 5.600 | 5.543 | 0.243 | 0.170 | 0.396 | 3.694 | 3.14e-01 |
| 26453 | 7.66 | 7.26 | 6.47 | 6.29 | 6.28 | 6.263 | 6.186 | 6.215 | 5.317 | 0.124 | 0.117 | 0.128 | 0.406 | 3.09e-01 |
| 26966 | 5.72 | 5.73 | 5.79 | 5.84 | 5.78 | 5.806 | 5.728 | 5.631 | 4.559 | 0.195 | 0.110 | 0.313 | 0.511 | 4.90e+00 |
| 27072 | 4.07 | 3.59 | 2.80 | 2.61 | 2.51 | 3.085 | 2.392 | 2.261 | 2.394 | 4.396 | 0.981 | 0.228 | 0.483 | 2.42e-30 |
| 27288 | 3.65 | 3.55 | 3.39 | 3.31 | 3.29 | 3.347 | 2.991 | 3.221 | 2.388 | 2.115 | 1.157 | 0.365 | 1.001 | 1.94e-01 |
| 27321 | 4.02 | 3.85 | 3.67 | 3.54 | 3.53 | 3.484 | 3.182 | 2.597 | 0.014 | 3.459 | 9.047 | 19.900 | 11.280 | 1.61e+00 |

(a) Table 1 - continued

| HIP | B | V | J | H | K | w1m | w2m | w3m | w4m | f12 | f25 | f60 | f100 | χ^2 |
|-------|-------|-------|------|------|------|--------|--------|-------|-------|-------|-------|-------|--------|----------|
| | mag | mag | mag | mag | mag | mag | mag | mag | mag | Jy | Jy | Jy | Jy | |
| 27980 | 8.28 | 7.65 | 6.49 | 6.23 | 6.15 | 6.169 | 6.069 | 6.170 | 6.084 | 0.169 | 0.150 | 0.940 | 14.910 | 2.51e-02 |
| 28103 | 4.05 | 3.71 | 3.06 | 2.98 | 2.99 | 2.021 | 1.749 | 2.905 | 2.792 | 2.878 | 0.726 | 0.212 | 1.648 | 3.72e-01 |
| 28230 | 7.83 | 7.55 | 7.01 | 6.93 | 6.88 | 6.851 | 6.853 | 6.834 | 5.708 | 0.087 | 0.061 | 0.193 | 0.435 | 3.54e-01 |
| 32480 | 5.82 | 5.24 | 4.41 | 4.07 | 4.13 | 3.872 | 3.439 | 3.954 | 3.825 | 1.463 | 0.412 | 0.381 | 1.020 | 5.04e+00 |
| 32775 | 6.57 | 6.11 | 5.30 | 5.13 | 5.02 | 5.003 | 4.794 | 5.053 | 4.990 | 0.391 | 0.084 | 0.183 | 1.643 | 6.71e-02 |
| 33690 | 7.60 | 6.81 | 5.46 | 5.10 | 4.99 | 4.959 | 4.698 | 4.980 | 4.672 | 0.400 | 0.267 | 0.180 | 1.137 | 4.66e-02 |
| 34276 | 6.51 | 6.52 | 6.49 | 6.48 | 6.48 | 6.486 | 6.411 | 6.489 | 5.853 | 0.124 | 0.097 | 0.203 | 0.940 | 1.73e-01 |
| 34819 | 6.25 | 5.85 | 5.20 | 4.98 | 4.83 | 4.904 | 4.661 | 4.877 | 4.771 | 0.551 | 0.109 | 0.151 | 0.699 | 7.91e-01 |
| 35550 | 3.87 | 3.50 | 2.82 | 2.60 | 2.56 | 1.491 | 1.004 | 2.622 | 2.526 | 3.903 | 0.834 | 0.256 | 0.622 | 7.28e-02 |
| 36906 | 8.34 | 7.68 | 6.49 | 6.23 | 6.16 | 6.135 | 6.036 | 6.145 | 6.053 | 0.176 | 0.135 | 0.145 | 0.567 | 1.44e-05 |
| 36948 | 8.96 | 8.23 | 6.91 | 6.58 | 6.46 | 6.448 | 6.369 | 6.416 | 5.644 | 0.357 | 0.250 | 0.613 | 9.612 | 5.86e-01 |
| 39757 | 3.29 | 2.83 | 2.17 | 2.08 | 2.02 | -0.227 | -0.061 | 1.961 | 1.856 | 7.199 | 1.757 | 0.397 | 1.145 | 2.84e-01 |
| 40938 | 7.64 | 7.24 | 6.34 | 6.15 | 6.09 | 6.089 | 5.932 | 6.097 | 5.986 | 0.168 | 0.149 | 0.165 | 1.297 | 3.08e-03 |
| 41152 | 5.64 | 5.52 | 5.25 | 5.29 | 5.25 | 5.255 | 5.092 | 5.270 | 4.838 | 0.372 | 0.140 | 0.177 | 0.494 | 5.09e-02 |
| 41307 | 3.90 | 3.91 | 4.12 | 4.09 | 4.08 | 3.927 | 3.556 | 3.925 | 3.429 | 1.087 | 0.394 | 0.280 | 1.874 | 2.86e+00 |
| 42028 | 5.81 | 5.80 | 5.77 | 5.82 | 5.73 | 5.795 | 5.707 | 5.819 | 5.697 | 0.202 | 0.129 | 0.144 | 0.593 | 4.20e-04 |
| 42430 | 5.77 | 5.05 | 4.05 | 3.59 | 3.59 | 3.446 | 3.183 | 3.480 | 3.405 | 1.784 | 0.380 | 0.151 | 0.549 | 3.10e+00 |
| 43970 | 5.37 | 5.22 | 4.91 | 4.97 | 4.87 | 4.894 | 4.527 | 4.927 | 4.593 | 0.470 | 0.223 | 0.319 | 0.796 | 1.97e-01 |
| 44001 | 5.89 | 5.68 | 5.27 | 5.21 | 5.16 | 5.158 | 4.978 | 5.195 | 4.886 | 0.324 | 0.235 | 0.391 | 1.386 | 9.43e-02 |
| 45758 | 6.88 | 6.62 | 6.15 | 6.04 | 5.96 | 6.032 | 5.886 | 6.015 | 5.917 | 0.216 | 0.118 | 0.192 | 0.586 | 1.44e-04 |
| 48164 | 7.43 | 7.20 | 6.75 | 6.68 | 6.63 | 6.637 | 6.611 | 6.666 | 6.177 | 0.119 | 0.136 | 0.243 | 0.628 | 1.60e-01 |
| 48541 | 7.75 | 7.59 | 7.21 | 7.20 | 7.19 | 7.095 | 7.164 | 7.103 | 6.071 | 0.113 | 0.128 | 0.193 | 0.487 | 7.59e-01 |
| 51438 | 4.76 | 4.72 | 4.75 | 4.71 | 4.57 | 4.555 | 4.348 | 4.609 | 4.531 | 0.606 | 0.155 | 0.145 | 1.092 | 2.11e+00 |
| 51658 | 4.94 | 4.72 | 4.12 | 4.06 | 4.20 | 4.121 | 3.875 | 4.210 | 4.169 | 0.919 | 0.185 | 0.397 | 0.955 | 3.04e+00 |
| 52462 | 8.59 | 7.72 | 6.18 | 5.77 | 5.66 | 5.613 | 5.509 | 5.629 | 5.556 | 0.219 | 0.083 | 0.248 | 0.984 | 8.08e-02 |
| 53524 | 7.59 | 7.36 | 6.91 | 6.87 | 6.79 | 6.717 | 6.745 | 6.692 | 5.475 | 0.281 | 0.250 | 0.601 | 1.830 | 2.01e+00 |
| 53910 | 2.37 | 2.34 | 2.27 | 2.36 | 2.29 | 1.156 | 0.845 | 2.461 | 2.138 | 4.795 | 1.387 | 0.627 | 1.000 | 3.98e+00 |
| 53911 | 11.64 | 10.92 | 8.22 | 7.56 | 7.30 | 7.009 | 6.878 | 4.540 | 1.516 | 0.613 | 2.435 | 4.105 | 4.900 | 1.78e+00 |
| 55505 | 10.04 | 8.89 | 6.40 | 5.76 | 5.59 | 5.496 | 5.344 | 3.110 | 0.202 | 1.981 | 9.443 | 7.895 | 4.565 | 5.34e-02 |
| 56253 | 6.38 | 6.12 | 5.66 | 5.60 | 5.56 | 5.589 | 5.435 | 5.604 | 5.435 | 0.243 | 0.114 | 0.141 | 0.863 | 3.59e-01 |
| 56675 | 6.00 | 5.64 | 4.97 | 4.92 | 4.70 | 4.718 | 4.483 | 4.698 | 4.606 | 0.568 | 0.250 | 0.275 | 7.545 | 8.22e-01 |
| 57632 | 2.23 | 2.14 | 1.85 | 1.93 | 1.88 | 0.461 | 0.129 | 2.056 | 1.698 | 7.067 | 2.323 | 1.027 | 1.120 | 7.91e+00 |
| 60074 | 7.64 | 7.04 | 5.87 | 5.61 | 5.54 | 5.522 | 5.357 | 5.540 | 5.182 | 0.259 | 0.135 | 0.705 | 0.909 | 1.73e-01 |
| 61174 | 4.69 | 4.30 | 3.61 | 3.37 | 3.37 | 2.685 | 2.912 | 3.308 | 2.752 | 2.242 | 0.770 | 0.308 | 0.803 | 1.56e-01 |
| 61498 | 5.78 | 5.78 | 5.78 | 5.79 | 5.77 | 5.368 | 5.399 | 5.024 | 1.222 | 0.433 | 3.379 | 7.359 | 3.814 | 1.69e+00 |
| 61782 | 8.14 | 7.99 | 7.64 | 7.59 | 7.58 | 7.523 | 7.564 | 7.053 | 3.913 | 0.094 | 0.266 | 0.368 | 1.155 | 1.53e-29 |
| 61960 | 4.96 | 4.88 | 4.99 | 4.76 | 4.68 | 4.649 | 4.298 | 4.700 | 4.259 | 0.547 | 0.235 | 0.270 | 0.579 | 2.64e+00 |
| 63584 | 6.44 | 6.01 | 5.19 | 5.05 | 5.00 | 4.983 | 4.757 | 5.033 | 4.914 | 0.362 | 0.150 | 0.130 | 0.424 | 6.06e-01 |
| 64375 | 6.68 | 6.49 | 6.12 | 6.02 | 6.01 | 5.980 | 5.906 | 6.014 | 5.631 | 0.196 | 0.182 | 0.330 | 0.796 | 6.75e-02 |
| 64921 | 7.28 | 7.07 | 6.65 | 6.59 | 6.57 | 6.634 | 6.303 | 6.435 | 6.529 | 0.116 | 0.062 | 0.192 | 1.779 | 3.37e+00 |
| 68101 | 6.78 | 6.00 | 4.57 | 4.02 | 3.99 | 4.008 | 3.792 | 4.020 | 3.965 | 1.047 | 0.194 | 0.382 | 10.230 | 1.81e-01 |
| 68593 | 7.72 | 7.16 | 6.16 | 5.94 | 5.88 | 5.882 | 5.794 | 5.883 | 5.701 | 0.187 | 0.079 | 0.150 | 0.305 | 1.85e-04 |
| 69682 | 9.56 | 8.89 | 7.65 | 7.38 | 7.27 | 7.166 | 7.250 | 7.230 | 6.678 | 0.133 | 0.128 | 0.207 | 0.404 | 5.72e-01 |
| 69732 | 4.27 | 4.18 | 3.98 | 4.03 | 3.91 | 3.922 | 3.758 | 4.118 | 3.611 | 1.151 | 0.356 | 0.472 | 1.000 | 3.74e+00 |

(a) Table 1 - continued

| HIP | B | V | J | H | K | w1m | w2m | w3m | w4m | f12 | f25 | f60 | f100 | χ^2 |
|--------|-------|------|-------|-------|------|--------|--------|-------|--------|--------|--------|-------|-------|----------|
| | mag | mag | mag | mag | mag | mag | mag | mag | mag | Jy | Jy | Jy | Jy | |
| 70090 | 4.02 | 4.05 | 4.11 | 3.98 | 4.07 | 4.063 | 3.851 | 4.092 | 3.914 | 0.953 | 0.313 | 0.171 | 1.233 | 3.46e-02 |
| 70344 | 7.80 | 7.21 | 6.12 | 5.87 | 5.79 | 5.816 | 5.714 | 5.773 | 5.274 | 0.185 | 0.089 | 0.182 | 0.586 | 1.89e-01 |
| 70952 | 6.53 | 6.10 | 5.26 | 5.09 | 5.01 | 5.447 | 5.194 | 5.965 | 5.151 | 0.349 | 0.084 | 0.344 | 0.525 | 1.78e+00 |
| 71075 | 3.23 | 3.04 | 2.65 | 2.57 | 2.51 | 1.378 | 1.247 | 2.621 | 2.470 | 3.937 | 0.980 | 0.366 | 0.496 | 1.87e+00 |
| 71284 | 4.83 | 4.47 | 3.56 | 3.46 | 3.34 | 3.478 | 3.146 | 3.507 | 3.444 | 1.606 | 0.413 | 0.140 | 0.452 | 1.78e+00 |
| 73049 | 5.37 | 5.32 | 5.22 | 5.22 | 5.13 | 5.173 | 5.010 | 5.193 | 5.031 | 0.332 | 0.155 | 0.190 | 1.342 | 5.66e-02 |
| 73145 | 8.07 | 7.88 | 7.60 | 7.56 | 7.52 | 7.514 | 7.523 | 6.922 | 4.273 | 0.156 | 0.186 | 0.684 | 1.324 | 6.53e-29 |
| 73473 | 4.91 | 4.91 | 4.71 | 4.71 | 4.62 | 4.602 | 4.405 | 4.681 | 4.584 | 0.623 | 0.282 | 0.141 | 0.974 | 5.57e-02 |
| 73512 | 10.17 | 9.13 | 7.19 | 6.69 | 6.58 | 6.577 | 6.555 | 6.572 | 6.527 | 0.123 | 0.122 | 0.130 | 0.405 | 9.28e-01 |
| 74596 | 5.34 | 5.28 | 5.09 | 5.15 | 5.11 | 5.094 | 4.926 | 5.150 | 4.939 | 0.348 | 0.100 | 0.142 | 0.601 | 4.97e-02 |
| 74946 | 2.88 | 2.87 | 2.52 | 2.53 | 2.53 | 1.597 | 1.539 | 2.731 | 2.732 | 3.372 | 0.763 | 0.416 | 5.406 | 1.78e+00 |
| 76127 | 4.01 | 4.14 | 4.43 | 4.47 | 4.43 | 4.412 | 4.133 | 4.394 | 4.228 | 0.623 | 0.182 | 0.162 | 0.452 | 3.43e-30 |
| 76267 | 2.25 | 2.22 | 2.25 | 2.39 | 2.21 | 0.942 | 0.935 | 2.263 | 1.940 | 5.807 | 1.686 | 0.705 | 0.869 | 3.12e-01 |
| 76375 | 8.60 | 7.65 | 6.01 | 5.62 | 5.50 | 5.698 | 5.325 | 5.511 | 5.466 | 0.211 | 0.070 | 0.142 | 0.614 | 1.11e+00 |
| 76635 | 8.05 | 7.50 | 6.50 | 6.25 | 6.18 | 6.202 | 6.130 | 6.201 | 5.985 | 0.199 | 0.114 | 0.131 | 0.936 | 7.64e-03 |
| 76736 | 6.53 | 6.45 | 6.30 | 6.34 | 6.27 | 6.270 | 6.219 | 6.160 | 5.010 | 0.263 | 0.250 | 0.482 | 4.657 | 4.30e+00 |
| 76829 | 5.05 | 4.64 | 4.02 | 3.73 | 3.80 | 3.681 | 3.087 | 3.650 | 3.521 | 1.425 | 0.693 | 0.661 | 2.368 | 4.87e+00 |
| 77163 | 5.61 | 5.57 | 5.47 | 5.46 | 5.43 | 5.402 | 5.258 | 5.428 | 4.997 | 0.330 | 0.124 | 0.283 | 0.920 | 8.59e+00 |
| 77542 | 7.21 | 7.11 | 6.87 | 6.86 | 6.82 | 6.061 | 6.095 | 4.701 | 1.861 | 0.533 | 1.819 | 5.335 | 3.548 | 1.78e+00 |
| 78554 | 4.89 | 4.82 | 5.01 | 4.66 | 4.62 | 4.647 | 4.455 | 4.653 | 4.574 | 0.577 | 0.145 | 0.190 | 0.749 | 3.26e+00 |
| 81126 | 4.19 | 4.20 | 4.42 | 4.34 | 4.05 | 4.173 | 3.903 | 4.175 | 4.099 | 0.937 | 0.270 | 0.265 | 0.651 | 4.49e+00 |
| 81641 | 5.77 | 5.77 | 5.75 | 5.79 | 5.74 | 5.824 | 5.712 | 5.792 | 5.340 | 0.207 | 0.111 | 0.226 | 1.189 | 3.55e-02 |
| 81800 | 7.02 | 6.48 | 5.44 | 5.17 | 5.15 | 5.168 | 4.994 | 5.166 | 5.023 | 0.321 | 0.073 | 0.116 | 0.640 | 1.02e-01 |
| 82405 | 6.72 | 6.32 | 5.46 | 5.29 | 5.18 | 5.188 | 5.019 | 5.202 | 5.123 | 0.381 | 0.262 | 0.295 | 1.148 | 8.22e-02 |
| 83480 | 6.89 | 6.70 | 6.30 | 6.25 | 6.22 | 6.190 | 6.092 | 6.190 | 6.048 | 0.156 | 0.104 | 0.321 | 2.245 | 1.96e-01 |
| 85157 | 5.93 | 5.70 | 5.24 | 5.21 | 5.18 | 5.178 | 5.028 | 5.167 | 4.018 | 0.356 | 0.212 | 0.536 | 1.086 | 2.54e-01 |
| 85537 | 5.65 | 5.41 | 4.81 | 4.88 | 4.80 | 4.777 | 4.572 | 4.802 | 4.599 | 0.572 | 0.258 | 0.366 | 2.093 | 2.38e-01 |
| 87108 | 3.79 | 3.75 | 3.59 | 3.66 | 3.62 | 3.677 | 3.356 | 3.646 | 3.118 | 1.417 | 0.525 | 1.269 | 3.733 | 1.21e-05 |
| 87558 | 6.20 | 5.77 | 5.21 | 4.83 | 4.71 | 4.737 | 4.453 | 4.717 | 4.576 | 0.544 | 0.250 | 0.380 | 1.265 | 3.00e+00 |
| 88399 | 7.47 | 7.01 | 6.16 | 6.02 | 5.91 | 5.758 | 5.703 | 5.799 | 4.940 | 0.208 | 0.158 | 0.647 | 2.631 | 2.83e+00 |
| 90185 | 1.76 | 1.79 | 1.73 | 1.77 | 1.77 | -0.704 | -0.165 | 1.763 | 1.681 | 8.460 | 2.047 | 0.586 | 2.616 | 7.25e-01 |
| 90936 | 6.65 | 6.22 | 5.42 | 5.28 | 5.20 | 5.206 | 5.053 | 5.224 | 5.082 | 0.292 | 0.139 | 0.504 | 1.029 | 1.32e-01 |
| 91262 | 0.03 | 0.03 | -0.18 | -0.03 | 0.13 | -2.034 | -2.082 | 0.017 | -0.157 | 41.530 | 11.310 | 9.568 | 7.912 | 9.42e-02 |
| 92024 | 4.98 | 4.78 | 4.38 | 4.25 | 4.30 | 4.335 | 4.065 | 3.624 | 2.355 | 1.518 | 1.092 | 0.306 | 0.991 | 8.61e-30 |
| 93542 | 4.71 | 4.74 | 4.72 | 4.96 | 4.75 | 4.794 | 4.526 | 4.723 | 3.792 | 0.577 | 0.306 | 0.321 | 1.119 | 6.98e-01 |
| 95261 | 5.05 | 5.03 | 5.10 | 5.15 | 5.01 | 5.059 | 4.822 | 4.725 | 3.261 | 0.481 | 0.491 | 0.495 | 0.435 | 1.45e-29 |
| 95270 | 7.52 | 7.04 | 6.20 | 5.98 | 5.91 | 5.887 | 5.810 | 5.894 | 3.952 | 0.164 | 0.248 | 1.855 | 1.719 | 1.51e-01 |
| 95619 | 5.65 | 5.66 | 5.67 | 5.66 | 5.68 | 5.677 | 5.559 | 5.612 | 4.579 | 0.190 | 0.199 | 0.412 | 0.942 | 1.79e+00 |
| 96468 | 4.28 | 4.36 | 4.44 | 4.42 | 4.48 | 4.549 | 4.256 | 4.593 | 4.511 | 0.609 | 0.166 | 0.265 | 1.804 | 8.80e-01 |
| 99273 | 7.66 | 7.18 | 6.32 | 6.09 | 6.08 | 6.062 | 5.882 | 5.995 | 4.056 | 0.111 | 0.339 | 0.711 | 0.328 | 1.96e-03 |
| 99473 | 3.17 | 3.24 | 3.29 | 3.28 | 3.29 | 3.390 | 3.024 | 3.435 | 3.350 | 1.745 | 0.447 | 0.204 | 0.941 | 1.78e+00 |
| 101612 | 5.04 | 4.75 | 4.28 | 4.02 | 4.04 | 4.060 | 3.582 | 4.045 | 3.865 | 1.016 | 0.264 | 0.522 | 1.798 | 3.38e-01 |
| 101769 | 4.07 | 3.64 | 2.87 | 2.76 | 2.64 | 1.584 | 0.844 | 2.634 | 2.518 | 4.069 | 0.921 | 0.229 | 1.066 | 8.24e-02 |

(a) Table 1 - continued

| HIP | B | V | J | H | K | w1m | w2m | w3m | w4m | f12 | f25 | f60 | f100 | χ^2 |
|--------|-------|------|------|------|------|-------|-------|-------|-------|-------|-------|-------|-------|----------|
| | mag | mag | mag | mag | mag | mag | mag | mag | mag | Jy | Jy | Jy | Jy | |
| 101800 | 5.47 | 5.42 | 5.41 | 5.37 | 5.30 | 5.324 | 5.134 | 5.326 | 4.968 | 0.251 | 0.124 | 0.177 | 1.077 | 8.79e-01 |
| 102409 | 10.28 | 8.81 | 5.44 | 4.83 | 4.53 | 4.499 | 3.999 | 4.312 | 4.137 | 0.760 | 0.300 | 0.270 | 0.687 | 1.13e-02 |
| 103752 | 6.46 | 6.36 | 6.13 | 6.11 | 6.05 | 6.056 | 5.921 | 6.085 | 6.121 | 0.146 | 0.103 | 0.244 | 0.638 | 2.07e-03 |
| 105570 | 5.22 | 5.16 | 5.09 | 4.98 | 4.92 | 4.885 | 4.699 | 4.966 | 4.793 | 0.459 | 0.251 | 0.274 | 1.925 | 3.40e-01 |
| 106741 | 7.59 | 7.19 | 6.38 | 6.25 | 6.18 | 6.192 | 6.066 | 6.185 | 5.927 | 0.159 | 0.113 | 0.199 | 0.520 | 7.66e-02 |
| 107022 | 7.83 | 7.07 | 5.73 | 5.41 | 5.27 | 5.309 | 5.121 | 5.306 | 5.209 | 0.315 | 0.107 | 0.174 | 0.987 | 1.23e-02 |
| 107412 | 7.13 | 6.69 | 5.87 | 5.69 | 5.59 | 5.573 | 5.452 | 5.629 | 5.481 | 0.249 | 0.194 | 0.228 | 0.491 | 1.02e-02 |
| 107649 | 6.17 | 5.57 | 4.72 | 4.31 | 4.24 | 4.116 | 3.817 | 4.156 | 4.065 | 0.805 | 0.216 | 0.245 | 1.000 | 5.01e+00 |
| 108809 | 7.13 | 6.63 | 5.70 | 5.44 | 5.39 | 5.338 | 5.180 | 5.393 | 5.251 | 0.287 | 0.152 | 0.137 | 0.680 | 1.33e-01 |

Notes: Col.(1): *Hipparcos* identification. Col.(2): B magnitude. Col.(3): V magnitude. Col.(4): J magnitude. Col.(5): H magnitude. Col.(6): K magnitude. Col.(7): *WISE* W1 magnitude. Col.(8): *WISE* W2 magnitude. Col.(9): *WISE* W3 magnitude. Col.(10): *WISE* W4 magnitude. Col.(11): *IRAS* 12 μm flux density. Col.(12): *IRAS* 25 μm flux density. Col.(13): *IRAS* 60 μm flux density. Col.(14): *IRAS* 100 μm flux density. Col.(15): The minimum χ^2 of SED fittings.

Table 5: The list of *WISE* 22 μm Excess Stars.

| HIP | Mid-IR excess | references |
|--------|---------------|------------|
| 5626 | no | |
| 7345 | yes | 1,2,3,4 |
| 11847 | yes | 2,3,5 |
| 16449 | yes | 2 |
| 18437 | yes | 2 |
| 22226 | yes | 2,5 |
| 23451 | no | 3,5 |
| 24528 | yes | 2 |
| 26453 | yes | 2,5 |
| 26966 | yes | 2 |
| 27288 | no | |
| 27321 | no | 1,3,4 |
| 28230 | yes | 2 |
| 36948 | no | 5 |
| 41307 | yes | |
| 48541 | yes | 2 |
| 53524 | no | 3 |
| 53911 | yes | |
| 55505 | yes | 1,3 |
| 61498 | no | 1,3 |
| 61782 | no | 1,4 |
| 73145 | no | 3,5 |
| 76736 | no | 3,5 |
| 85157 | no | |
| 88399 | no | 3 |
| 92024 | yes | 4 |
| 93542 | yes | 2 |
| 95261 | yes | 1,2 |
| 95270 | yes | 2,3,5 |
| 99273 | no | 3 |
| 116431 | no | 2 |

Notes: Col.(1): *Hipparcos* identification. Col.(2): Check the 22 μm excess by *IRAS* 100 μm background level lower than 5 MJy/sr or not, yes means the excess should be true and no means the excess may not be true. Col.(3): References - 1. [Fujiwara et al. 2013](#); 2. [Wu et al. 2013](#); 3. [Liu et al. 2014](#); 4. [Ishihara et al. 2017](#); 5. [Ballering et al. 2018](#).

Table 6: The Dust Properties of Group I Stars.

| HIP | T-Rhee(K) | f-Rhee | T(K) | f |
|--------|-----------|----------|------|----------|
| 4267 | 85 | 8.80e-05 | 73 | 7.13e-05 |
| 6686 | 85 | 5.90e-06 | 105 | 6.17e-06 |
| 8122 | 85 | 4.70e-04 | 66 | 3.40e-04 |
| 9570 | 85 | 1.00e-04 | 69 | 8.16e-05 |
| 11486 | 85 | 1.10e-04 | 85 | 1.13e-04 |
| 11847 | 85 | 1.70e-03 | 83 | 1.43e-03 |
| 13005 | 85 | 1.10e-03 | 52 | 7.56e-04 |
| 18437 | 85 | 2.60e-04 | 105 | 2.93e-04 |
| 18859 | 85 | 1.30e-04 | 94 | 1.38e-04 |
| 18975 | 85 | 8.90e-05 | 69 | 7.45e-05 |
| 20635 | 85 | 4.70e-05 | 81 | 4.33e-05 |
| 23451 | 85 | 5.40e-03 | 87 | 4.68e-03 |
| 25790 | 85 | 2.50e-04 | 55 | 1.21e-04 |
| 26966 | 85 | 2.00e-04 | 99 | 1.76e-04 |
| 34276 | 85 | 2.00e-04 | 73 | 1.72e-04 |
| 36906 | 85 | 4.30e-04 | 50 | 2.95e-04 |
| 39757 | 85 | 5.40e-06 | 128 | 1.03e-05 |
| 40938 | 85 | 3.50e-04 | 53 | 2.29e-04 |
| 42028 | 85 | 7.10e-05 | 59 | 5.16e-05 |
| 43970 | 85 | 1.00e-04 | 73 | 6.48e-05 |
| 44001 | 85 | 2.20e-04 | 66 | 1.25e-04 |
| 45758 | 85 | 2.70e-04 | 51 | 1.82e-04 |
| 48164 | 85 | 5.50e-04 | 63 | 2.97e-04 |
| 48541 | 85 | 4.80e-04 | 76 | 2.85e-04 |
| 51438 | 85 | 2.40e-05 | 79 | 2.49e-05 |
| 53524 | 85 | 1.50e-03 | 69 | 7.55e-04 |
| 56253 | 85 | 1.00e-04 | 61 | 6.66e-05 |
| 61960 | 85 | 6.20e-05 | 94 | 7.11e-05 |
| 64375 | 85 | 3.90e-04 | 64 | 3.04e-04 |
| 69682 | 85 | 2.10e-03 | 62 | 1.43e-03 |
| 70344 | 85 | 3.80e-04 | 80 | 3.36e-04 |
| 73049 | 85 | 7.40e-05 | 67 | 5.67e-05 |
| 73512 | 85 | 1.20e-03 | 54 | 7.25e-04 |
| 76635 | 85 | 3.90e-04 | 64 | 2.96e-04 |
| 82405 | 85 | 3.00e-04 | 53 | 1.81e-04 |
| 83480 | 85 | 4.30e-04 | 52 | 2.14e-04 |
| 87108 | 85 | 7.80e-05 | 81 | 7.68e-05 |
| 87558 | 85 | 2.50e-04 | 69 | 2.00e-04 |
| 95619 | 85 | 2.00e-04 | 88 | 1.71e-04 |
| 99473 | 85 | 6.60e-06 | 92 | 7.22e-06 |
| 103752 | 85 | 2.50e-04 | 52 | 1.56e-04 |
| 105570 | 85 | 8.80e-05 | 68 | 6.86e-05 |
| 106741 | 85 | 4.00e-04 | 61 | 2.01e-04 |
| 110867 | 85 | 7.10e-04 | 59 | 5.13e-04 |
| 116431 | 85 | 7.40e-04 | 84 | 5.23e-04 |

Table 7: The Dust Properties of Group II Stars.

| HIP | T-Rhee(K) | f-Rhee | T(K) | f |
|-------|-----------|----------|------|----------|
| 746 | 120 | 2.50e-05 | 109 | 1.85e-05 |
| 1185 | 40 | 4.30e-04 | 36 | 2.67e-04 |
| 5626 | 75 | 1.50e-04 | 83 | 1.40e-04 |
| 6878 | 45 | 2.10e-04 | 50 | 1.88e-04 |
| 7345 | 80 | 7.90e-04 | 76 | 7.90e-04 |
| 7805 | 70 | 3.70e-04 | 74 | 2.69e-04 |
| 7978 | 65 | 4.20e-04 | 68 | 3.63e-04 |
| 8241 | 75 | 6.40e-05 | 76 | 7.03e-05 |
| 10054 | 60 | 8.70e-05 | 66 | 5.20e-05 |
| 10670 | 75 | 7.20e-05 | 74 | 5.57e-05 |
| 11360 | 65 | 5.10e-04 | 68 | 4.74e-04 |
| 12361 | 40 | 5.90e-04 | 37 | 3.22e-04 |
| 12964 | 55 | 2.00e-04 | 54 | 1.27e-04 |
| 13141 | 55 | 6.40e-05 | 83 | 4.81e-05 |
| 14576 | 250 | 1.70e-05 | 138 | 7.79e-06 |
| 15197 | 95 | 2.50e-05 | 79 | 4.61e-05 |
| 16449 | 60 | 4.90e-04 | 66 | 4.71e-04 |
| 16537 | 40 | 8.30e-05 | 53 | 7.52e-05 |
| 19893 | 80 | 2.30e-05 | 74 | 3.81e-05 |
| 21604 | 75 | 3.80e-04 | 54 | 1.89e-04 |
| 22226 | 65 | 8.80e-04 | 70 | 6.51e-04 |
| 22439 | 40 | 2.30e-04 | 62 | 1.21e-04 |
| 22845 | 80 | 8.40e-05 | 88 | 8.24e-05 |
| 24528 | 100 | 1.70e-04 | 94 | 1.82e-04 |
| 25197 | 120 | 7.00e-05 | 86 | 5.06e-05 |
| 26453 | 90 | 2.80e-04 | 97 | 3.21e-04 |
| 27072 | 90 | 7.70e-06 | 133 | 1.93e-05 |
| 27288 | 220 | 1.30e-04 | 175 | 8.09e-05 |
| 27321 | 110 | 2.60e-03 | 109 | 2.65e-03 |
| 27980 | 70 | 2.80e-03 | 38 | 2.62e-03 |
| 28103 | 185 | 2.00e-05 | 114 | 1.29e-05 |
| 28230 | 90 | 6.10e-04 | 82 | 4.35e-04 |
| 32480 | 60 | 8.90e-05 | 82 | 1.29e-04 |
| 32775 | 45 | 1.60e-04 | 54 | 1.07e-04 |
| 33690 | 80 | 2.00e-04 | 82 | 2.31e-04 |
| 34819 | 45 | 1.00e-04 | 72 | 7.69e-05 |
| 35550 | 60 | 8.90e-06 | 82 | 1.13e-05 |
| 36948 | 60 | 2.60e-03 | 63 | 2.31e-03 |
| 41152 | 80 | 5.20e-05 | 85 | 5.23e-05 |
| 41307 | 130 | 4.10e-05 | 128 | 4.36e-05 |
| 42430 | 80 | 3.20e-05 | 119 | 5.21e-05 |
| 51658 | 40 | 1.10e-04 | 37 | 6.79e-05 |
| 52462 | 45 | 6.70e-04 | 50 | 5.43e-04 |
| 53910 | 120 | 1.20e-05 | 94 | 1.22e-05 |
| 55505 | 160 | 1.10e-01 | 136 | 6.59e-02 |
| 56675 | 50 | 1.40e-04 | 65 | 6.84e-05 |

(a) Table 4 - continued

| HIP | T-Rhee(K) | f-Rhee | T(K) | f |
|--------|-----------|----------|------|----------|
| 61174 | 180 | 1.20e-04 | 156 | 1.05e-04 |
| 61498 | 110 | 4.40e-03 | 108 | 4.22e-03 |
| 61782 | 130 | 2.50e-03 | 119 | 2.41e-03 |
| 63584 | 100 | 1.00e-04 | 55 | 4.43e-05 |
| 64921 | 80 | 3.40e-04 | 55 | 2.10e-04 |
| 68101 | 45 | 2.50e-04 | 71 | 1.93e-04 |
| 68593 | 60 | 1.40e-04 | 62 | 2.19e-04 |
| 69732 | 100 | 5.20e-05 | 84 | 4.59e-05 |
| 70090 | 120 | 2.10e-05 | 89 | 1.53e-05 |
| 71075 | 55 | 1.00e-05 | 69 | 8.35e-06 |
| 73145 | 90 | 3.10e-03 | 91 | 2.95e-03 |
| 73473 | 150 | 7.20e-05 | 69 | 1.79e-05 |
| 74596 | 65 | 3.30e-05 | 74 | 2.97e-05 |
| 76127 | 75 | 2.00e-05 | 99 | 7.85e-06 |
| 76267 | 190 | 2.40e-05 | 127 | 1.97e-05 |
| 76375 | 29 | 7.90e-04 | 28 | 3.97e-04 |
| 76736 | 140 | 1.20e-04 | 79 | 3.99e-04 |
| 76829 | 75 | 1.20e-04 | 77 | 1.29e-04 |
| 77163 | 40 | 1.40e-04 | 72 | 1.16e-04 |
| 78554 | 45 | 4.60e-05 | 76 | 3.73e-05 |
| 81126 | 80 | 3.00e-05 | 80 | 2.57e-05 |
| 81641 | 95 | 1.20e-04 | 74 | 9.24e-05 |
| 81800 | 55 | 8.30e-05 | 66 | 9.49e-05 |
| 85157 | 90 | 2.70e-04 | 92 | 2.14e-04 |
| 85537 | 70 | 6.80e-05 | 63 | 6.52e-05 |
| 88399 | 70 | 1.00e-03 | 72 | 6.40e-04 |
| 90185 | 100 | 4.50e-06 | 115 | 4.80e-06 |
| 90936 | 50 | 4.60e-04 | 52 | 2.25e-04 |
| 91262 | 80 | 2.10e-05 | 76 | 1.77e-05 |
| 92024 | 320 | 8.10e-04 | 269 | 6.18e-04 |
| 93542 | 120 | 9.70e-05 | 116 | 8.99e-05 |
| 95261 | 150 | 2.10e-04 | 126 | 2.17e-04 |
| 95270 | 75 | 3.50e-03 | 75 | 3.38e-03 |
| 96468 | 60 | 3.50e-05 | 70 | 2.26e-05 |
| 99273 | 95 | 1.40e-03 | 91 | 1.79e-03 |
| 101612 | 65 | 1.10e-04 | 71 | 1.00e-04 |
| 101769 | 130 | 1.60e-05 | 116 | 1.06e-05 |
| 101800 | 100 | 3.90e-05 | 83 | 6.34e-05 |
| 102409 | 50 | 3.60e-04 | 60 | 3.99e-04 |
| 107022 | 80 | 2.90e-04 | 55 | 2.35e-04 |
| 107412 | 55 | 2.70e-04 | 58 | 2.33e-04 |
| 107649 | 55 | 1.20e-04 | 84 | 1.12e-04 |
| 108809 | 75 | 7.30e-05 | 67 | 1.33e-04 |
| 109857 | 65 | 1.60e-04 | 67 | 1.39e-04 |
| 111278 | 55 | 9.30e-05 | 47 | 8.48e-05 |
| 113368 | 65 | 8.00e-05 | 57 | 5.72e-05 |